ChemComm

COMMUNICATION

View Article Online
View Journal | View Issue

Cite this: *Chem. Commun.*, 2026, **62**, 218

Received 15th September 2025,
Accepted 4th November 2025

DOI: 10.1039/d5cc05315c

rsc.li/chemcomm

Excited-state structural conformations of Fe-amido photosensitizers revealed by picosecond X-ray absorption spectroscopy

Maxime Sauvan,[a] Asterios Charisiadis,[a] Lucia Velasco,[ab] Ana Martinez,[a] Issiah B. Lozada,[c] Xiaoyi Zhang,[d] David E. Herbert *[c] and Dooshaye Moonshiram *[a]

Ultrafast X-ray spectroscopy and modelling were used to characterize distortions in the photo-generated quintet state of Fe sensitizers bearing hybrid N-heterocycle/amido ligands. Photoexcitation induces a 0.10–0.35 Å Fe–N elongation that is smaller for *d*(Fe–N_{amido}) compared to *d*(Fe-$N_{heterocycle}$), suggesting that the partial expansion of the Fe–N bonds involving the N-heterocyclic ligands is critical to the rapid population of ligand-field states.

The past decade has seen extensive efforts re-dedicated towards the development of cost-effective and environmentally friendly replacements for precious-metal photosensitizers.[1,2] The challenge with abundant 3d elements is replicating the ability of 4d and 5d transition metal complexes to access long-lived charge-transfer (*e.g.*, ^{3}MLCT) states,[3] which tend to be prized for bimolecular photochemical reactivity.[4] Iron (Fe) is one of the most appealing targets, thanks to its high abundance in the Earth's crust[5] and rich coordination chemistry.[6] The design of Fe-based photosensitizers with properties competitive to analogues of Ru, *inter alia*, has to date met with the most success through the use of Fe^{III} complexes with strong-field ligands that can access doublet ligand-to-metal charge-transfer (^{2}LMCT) excited states.[7] Combining carbene or cyclometallating aryl donors with d^5 electronic configurations destabilizes otherwise deactivating metal-centred (MC) excited states, enabling observable luminescence[8,9] and lifetimes long enough for expansive photoreactivity.[10–12]

With limited exceptions, similar success with d^6 Fe^{II} MLCT excited states has remained elusive but with tantalizing hints that such chemistry might be possible with a more developed understanding of the interplay between ligand design and excited-state properties. With these ideas in mind, we undertook a study of the excited-state structural dynamics of two Fe(II) amido sensitizer candidates [(^{R}L)$_2$Fe, R = CF_3, Cl; Fig. 1] that exhibit panchromatic absorption and nanosecond excited-state lifetimes.[13]

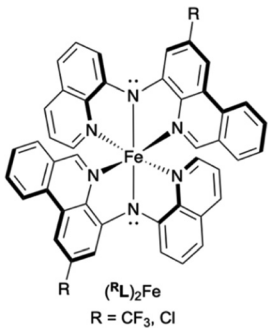

Fig. 1 Structures of the Fe photosensitizers (^{R}L)$_2$Fe (R = CF_3, Cl).

Both (^{R}L)$_2$Fe complexes bear divalent Fe^{II} ions ligated by tridentate diarylamido ligands with supporting benzannulated phenanthridine (phen) and quinoline (quin) N-heterocyclic donor arms. The amido donors, in particular, are thought to be responsible for the unique absorptive properties of the complexes.[14] The highly covalent Fe–N_{amido} bonds reduce electron repulsion, counteracting the impact of what are otherwise 'weak-field' ligands on the excited-state ordering at the ground-state geometry.[15] Femtosecond time-resolved X-ray emission (XES) spectroscopy nevertheless showed that photoexcitation populates a low-lying ligand-field quintet (^{5}MC) excited-state,[16] corroborated by subsequent wide-band optical transient absorption experiments.[17] To leverage this increasing understanding of the promise and limitations of these ligand designs, we sought to further understand the structural changes that accompany light absorption, specifically, the differences (if any) that might be observed in the three distinct Fe–N bond types: the dative Fe–N_{phen} and Fe–N_{quin} bonds, and the highly covalent Fe–N_{amido} bonds. Ultrafast X-ray absorption

[a] *Instituto de Ciencia de Materiales de Madrid Consejo Superior de Investigaciones Cientificas Sor Juana Ines de la Cruz, 3, Madrid 28049, Spain. E-mail: dooshaye.moonshiram@csic.es*
[b] *Departamento de Quimica Fisica, Universidad Complutense de Madrid, Avenida Complutense s/n, Madrid, E-28040, Spain*
[c] *Department of Chemistry, University of Manitoba, Winnipeg, Manitoba, Canada. E-mail: david.herbert@umanitoba.ca*
[d] *X-ray Science Division, Argonne National Laboratory, 9700 S. Cass Avenue, Lemont IL, USA*

spectroscopic techniques, which can directly probe electronic and nuclear dynamics around a metal, have helped significantly advance our mechanistic understanding of photochemical processes, solar energy conversion pathways, and ultrafast electron transfer dynamics.[18–22] Time-resolved X-ray scattering has further been used to investigate changes in average metal–ligand bond distances, as well as to probe the rearrangement of the ligand cage and the hydrodynamic response of the surrounding solvent.[23,24] In this work, we focused on picosecond time-resolved X-ray absorption spectroscopy (tr-XAS) studies of $(^{R}L)_2Fe$, complemented by time-dependent density functional theory (TD-DFT) and DFT calculations, to determine the structural configurations of the ^{5}MC states and critical geometrical factors influencing their fast relaxation to their respective ground states.

Steady-state X-ray absorption near-edge structure (XANES) and extended X-ray absorption fine-structure (EXAFS) analyses (Fig. 2) were first carried out on $(^{CF_3}L)_2Fe$ and $(^{Cl}L)_2Fe$ in acetonitrile solution. Both complexes display identical features in the rising and main-edge regions from 7110 to 7170 eV (Fig. 2A), indicating similar local coordination environments and geometrical conformations. The EXAFS spectra contain a prominent peak (labelled **I** in Fig. 2B) corresponding to the averaged Fe–N bond distances. The EXAFS fits for the extraction of the actual bond distances of both complexes are shown in the inset of Fig. 2B and Fig. S1 and Table S1. Analysis of the EXAFS spectra clearly resolves six Fe–N bond lengths at 1.92 ± 0.01 Å for $(^{CF_3}L)_2Fe$ and 1.94 ± 0.01 Å for $(^{Cl}L)_2Fe$ (Table S1 and Fig. S1A, B). The experimental EXAFS results for the averaged Fe–N distances of $(^{R}L)_2Fe$ are in perfect agreement with those derived from previous X-ray diffraction analysis (XRD).[13,15]

Density functional theory (DFT) geometry optimization calculations were carried out using the PBE0 exchange–correlation functional[25] as previously reported[16] (see the SI, for more details, including Table S2). The experimental EXAFS trends lie between 0.01 and 0.03 Å of the average computed Fe–N bond lengths (Table S2 and Fig. S1A, B). The experimental EXAFS profiles closely align with those calculated from the DFT-optimized structures (Fig. S2 and Table S2), reinforcing the reliability of our theoretical approach. The Fe–N bond distances to the heterocyclic N-atoms ($N_{phen/quin}$) are comparable in both complexes. This indicates that substituting the 2-position of the phenanthridinyl unit with either trifluoromethyl or chloride groups does not significantly alter the coordination environment of the Fe centre, consistent with previous observations.[13,15]

Time-resolved picosecond XAS was then employed to capture snapshots of the excited-state conformations of $(^{CF_3}L)_2Fe$ and $(^{Cl}L)_2Fe$. In this pump–probe configuration, an ultrafast laser pulse (pump) photoexcites the molecular complexes, initiating transient electronic and structural changes. These dynamics are subsequently interrogated using a time-delayed X-ray pulse (the probe), tracking the complexes' spectroscopic response on the pico- to microsecond timescales. Solutions of $(^{CF_3}L)_2Fe$ and $(^{Cl}L)_2Fe$ were thus pumped using 400 nm excitation and the tr-XAS spectra were collected both before (laser-off) and after (laser-on) laser excitation (Fig. 3). By subtracting the laser-off spectrum from the laser-on spectrum at each pump–probe delay, we obtained a time-resolved transient signal that reveals transient features associated with the photoinduced electronic and structural dynamics.

The transient signals monitored for both photosensitizers within an X-ray pulse duration of 80 ps exhibit a prominent feature at 7126.9 eV, accompanied by a shoulder near 7137.5 eV, indicative of excited-state formation (Fig. 3). Additionally, a broad bleach centred around 7147.7 eV is observed, corresponding to depopulation of the Fe^{II} ground state. The MLCT states of polypyridyl Fe coordination complexes typically decay through low-lying energetic pathways involving their triplet and quintet MC states;[26] the decay cascades of $(^{CF_3}L)_2Fe$ and $(^{Cl}L)_2Fe$ similarly involve a rapid ^{1}MLCT→^{3}MLCT→^{3}MC→^{5}MC trajectory prior to ground-state recovery.[16,17] At 80 ps, both trXES[16] and wide-band optical TA experiments[17] indicate that the quintet ^{5}MC excited state is fully populated. Time-dependent DFT (TD-DFT) XANES

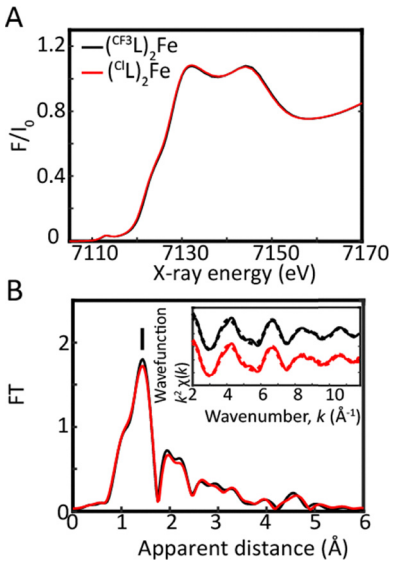

Fig. 2 (a) Normalized Fe K-edge XANES of 0.8 mM solutions of $(^{CF_3}L)_2Fe$ (black) and $(^{Cl}L)_2Fe$ (red) in CH_3CN. (b) Fourier transforms of k^2-weighted Fe EXAFS for $(^{CF_3}L)_2Fe$ (black) and $(^{Cl}L)_2Fe$ (red); inset: $k^2[\chi(k)]$ weighted traces as a function of k, the photoelectron wavevector (solid lines) and fitted (dashed lines) from 2 to 11.8 Å^{-1}.

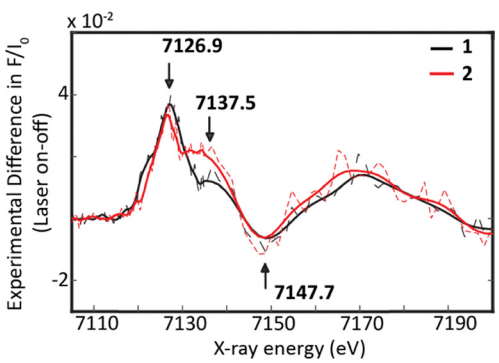

Fig. 3 The time-resolved XAS spectra (laser on−off) corresponding to the excited states of $(^{CF_3}L)_2Fe$ (black) and $(^{Cl}L)_2Fe$ (red) in 0.8 mM CH_3CN solutions at a delay of 80 ps between pump and probe pulses. Dashed lines indicate the raw data, while bold lines represent the smoothed spectra.

simulations in the pre-edge and rising edge regions of both the triplet and quintet excited-state geometries confirm this assignment for the experimental transient signal. Specifically, the TD-DFT XANES profiles simulated for the ^{3}MC excited state predict a positive shift in the rising edge, opposite to the negative shift in the rising edge energy calculated for ^{5}MC (Fig. S3) and observed in the time-resolved experiment (see positive feature at ~7120 eV in Fig. 3).

Indeed, comparing the 'laser on' and 'laser off' XANES spectra for $(^{CF_3}L)_2Fe$ shows a clear energy shift of −0.45 eV ('laser on': 7125.73 *vs.* 'laser off': 7126.18 eV) at roughly half-height/0.6 normalized absorption (Fig. S4A). For $(^{Cl}L)_2Fe$, we record a shift of −0.40 eV ('laser on': 7125.78 *vs.* 'laser off': 7126.18 eV; Fig. S4B). We estimated the percentage population of the ^{5}MC state generated by photoexcitation using two approaches. First, we compared the energy shift observed in the laser on/off spectra of $(^{Cl}L)_2Fe$ to that observed for the singlet/quintet states of a reference pseudo-octahedral ferrous complex, for which a shift of −2.093 eV ('laser off': 7124.89 eV *vs.* 'laser on': 7122.80 eV) was observed (Fig. S5).[27] Taking a simple ratio of this shift compared to the experimentally observed shifts produces estimates of excited state populations of 22% for $(^{CF_3}L)_2Fe$ and 19% for $(^{Cl}L)_2Fe$. Second, we considered a set of experimental parameters including molar absorptivity, laser spot size, and pulse energy (see the SI, Table S3). Using this approach, we estimated an ^{5}MC excited state population of 26% for $(^{CF_3}L)_2Fe$ and 23% for $(^{Cl}L)_2Fe$. Combining these two estimates, we bracket the excited state population at 24 ± 2% for $(^{CF_3}L)_2Fe$ and 21 ± 2% for $(^{Cl}L)_2Fe$. These values were subsequently used to plot the actual or reconstructed spectra of the pure excited state (Fig. 4C and D).

The reconstructed XANES spectrum of $(^{CF_3}L)_2Fe$ contains two weak pre-edge transitions at 7112.4 eV and 7117.2 eV, while that of $(^{Cl}L)_2Fe$ shows similar transitions at 7113.0 eV and 7116.0 eV (Fig. 4A and B, insets). Those features are consistent with previously investigated Fe-based high-spin quintet (^{5}MC) states.[27] The TD-DFT calculated XANES spectra of the quintet excited state contain two distinct pre-edge features at approximately the same energies (Fig. S6). The transient EXAFS on/off spectra of both complexes display two prominent peaks (**II** and **III**; Fig. 4C and D). These represent the contributions of two distinct sets of Fe–N bonds in the excited state. Analysis of the spectrum within the first coordination sphere of $(^{CF_3}L)_2Fe$ clearly resolves two distinct sets of Fe–N bond lengths at 2.01 ± 0.02 Å and 2.27 ± 0.02 Å, corresponding to two and four Fe–N interactions, respectively (Table S1 and Fig. S7). These measurements were consistent across a range of excited-state populations (22–26%; Fig. 4c and Table S2, Fig. S7). Analysis of the corresponding spectra of $(^{Cl}L)_2Fe$ similarly shows two Fe–N bond distances at 2.05 ± 0.03 Å and four Fe–N bonds at 2.29 ± 0.03 Å for excited state populations ranging from 19 to 23% (Fig. 4d and Table S1, Fig. S8).

EXAFS itself cannot, of course, resolve the directionality of bond elongation. We assign the shorter distances to the two highly covalent Fe–N_{amido} bonds and the four longer distances to the Fe–$N_{phen/quin}$ interactions. This assignment is consistent with the DFT-calculated geometries of the quintet excited states (Table S2 and Appendix A). This assignment is also supported

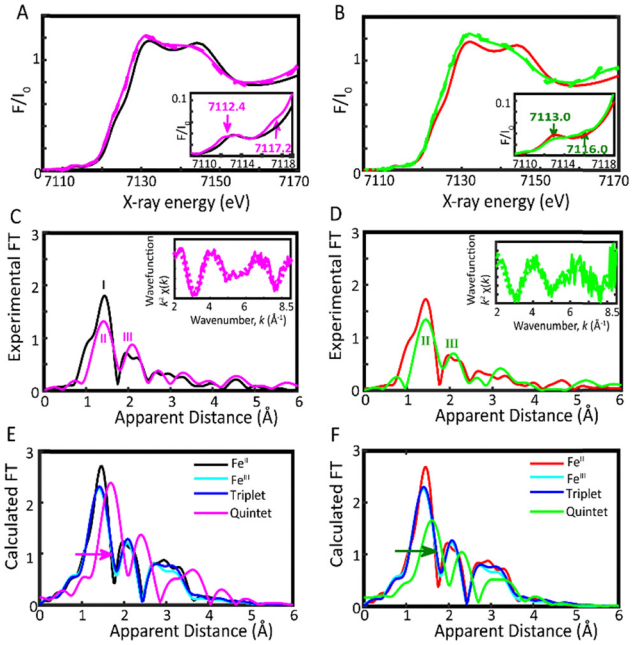

Fig. 4 Normalized Fe K-edge XANES of the laser off spectrum (black) and reconstructed excited state of (a) $(^{CF_3}L)_2Fe$ assuming a percentage excited state of 24% (in magenta) and (b) $(^{Cl}L)_2Fe$ assuming a percentage excited state of 21% (in green); dashed lines and bold lines indicate the raw and smoothed data; insets show a magnification of the pre-edge and rising edge regions. Experimental Fourier transforms of k^2-weighted Fe EXAFS of the laser of (in black) and reconstructed excited state of (c) $(^{CF_3}L)_2Fe$ and (d) $(^{Cl}L)_2Fe$; insets: $k^2[\chi(k)]$ weighted traces as a function of k, the photoelectron wavevector (solid lines) and fitted (dashed lines) from 2 to 8.5 Å^{-1}. The calculated EXAFS spectra for a ground-state singlet, Fe^{III}, triplet and quintet excited states of (e) $(^{CF_3}L)_2Fe$ and (f) $(^{Cl}L)_2Fe$ using atomic coordinates obtained from DFT simulations.

by the solid-state structure of an analogous $(^{CF_3}L')_2Fe$ complex with a high-spin quintet electronic ground-state.[16] In such high-spin ground-state analogues of $(^{R}L)_2Fe$, installation of methyl groups adjacent to the phenanthridine N-donors leads to the stabilization of an $S = 2$ ground state through elongation of the Fe–$N_{phen/quin}$ distances [Δd(HS-LS)/Å = 0.273 (Fe–N_{phen}), 0.201 (Fe–N_{quin})]. Lengthening these four specific Fe–N bonds, particularly the Fe–N_{phen} interactions where steric strain is the highest, is enough to induce spin-crossover and strong Fe–N_{amido} interactions are retained [Δd(HS-LS)/Å = 0.146].[16] The EXAFS-fitted values for the two sets of Fe–N bonds for both $(^{CF_3}L)_2Fe$ and $(^{Cl}L)_2Fe$ are in good agreement with each other and lie between 0.09 and 0.11 Å of their DFT-optimized structures (Table S2).

The elongation of the averaged Fe–N bond distances observed in the quintet excited states, along with the corresponding changes in the experimental EXAFS spectra for $(^{CF_3}L)_2Fe$ (Fig. 4C) and $(^{Cl}L)_2Fe$ (Fig. 4D), additionally shows a strong correlation with the EXAFS profiles calculated from the DFT-optimized geometries of a quintet excited state (Fig. 4E and F). Thus, upon light excitation, both $(^{CF_3}L)_2Fe$ and $(^{Cl}L)_2Fe$ undergo rapid deactivation of initially formed charge-separated states, favouring d-orbital rearrangements within the 80 ps X-ray pulse duration. A bond elongation in the first coordination sphere from the ground to the quintet excited state is observed, ranging from 0.09 ± 0.03 to 0.35 ± 0.03 Å for $(^{CF_3}L)_2Fe$ and

0.11 ± 0.04 to 0.35 ± 0.04 Å for $(^{Cl}L)_2Fe$ (Table S1). The Fe–N bond length changes obtained for the ^{5}MC states are consistent with their relaxed DFT-optimized geometries (Table S2 and Fig. S9). Bond elongation comparable to that observed for the $Fe–N_{phen/quin}$ distances (~0.22–0.34 Å) has also been seen in an Fe^{II} spin crossover complex featuring macrocyclic ligands.[27] Though $(^{CF_3}L)_2Fe$ contains more electron-withdrawing CF_3 groups compared to the chloride substituents in $(^{Cl}L)_2Fe$, potentially influencing the electron distribution about the metal, both complexes exhibit similar Fe–N bond lengths in their ground and excited states. This observation is likely due to the positioning of the CF_3 substituents on the 2-phenanthridinyl unit, spatially distant from the Fe centre (Fig. 1). As a result, the local structural conformation remains largely unaffected, as confirmed through EXAFS analysis.

The asymmetry observed in the experimental EXAFS and DFT optimizations shows that elongation of the four Fe–N bonds associated with the phenanthridine and quinoline N-heterocyclic donors is sufficient for electron-transfer into the ligand-field manifold, consistent with ground-state models of the ^{5}MC excited state.[16] The structural distortions between the ground and excited states suggest that a partial expansion of the Fe–N bonds involving the quinoline and phenanthridine ligands alone can facilitate rapid relaxation back to the ground state. This points to an important potential design strategy for elongating charge-transfer lifetimes in this particular class of panchromatic Fe-based photosensitizers, where the amido donors have proven critical to strong, broad light absorption.[13,14] For example, ligand design strategies that replace quinoline/phenanthridine donors with those that can form stronger metal–ligand bonds might suppress the formation of low-lying MC states[28,29] without sacrificing the unique characteristics of Fe-amido chromophores. Experimental work to realize such strategies is currently underway.

We acknowledge funding from Ramon y Cajal grant RYC2020-029863-I and support from the Natural Sciences and Engineering Research Council of Canada (RGPIN-2022-04501). This research used the Advanced Photon Source supported by the US Department of Energy (Contract No. DE-AC02-06CH11357).

Conflicts of interest

There are no conflicts to declare.

Data availability

The data supporting this article have been included as part of the supplementary information (SI). Supplementary information: Experimental section, EXAFS analysis, DFT optimizations, and TD-DFT XANES simulations. See DOI: **https://doi.org/10.1039/d5cc05315c**.

Notes and references

1 O. S. Wenger, *J. Am. Chem. Soc.*, 2018, **140**, 13522–13533.
2 N. Sinha and O. S. Wenger, *J. Am. Chem. Soc.*, 2023, **145**, 4903–4920.
3 G. Morselli, C. Reber and O. S. Wenger, *J. Am. Chem. Soc.*, 2025, **147**, 11608–11624.
4 B. Dietzek-Ivanšić, K. Heinze, S. Rau, O. S. Wenger and A. Pannwitz, *Coord. Chem. Rev.*, 2025, **526**, 216362.
5 A. A. Yaroshevsky, *Geochem. Int.*, 2006, **44**, 48–55.
6 P. Dierks, Y. Vukadinovic and M. Bauer, *Inorg. Chem. Front.*, 2022, **9**, 206–220.
7 Y. Liu, P. Persson, V. Sundström and K. Wärnmark, *Acc. Chem. Res.*, 2016, **49**, 1477–1485.
8 P. Chábera, Y. Liu, O. Prakash, E. Thyrhaug, A. E. Nahhas, A. Honarfar, S. Essén, L. A. Fredin, T. C. Harlang, K. S. Kjær, K. Handrup, F. Ericson, H. Tatsuno, K. Morgan, J. Schnadt, L. Häggström, T. Ericsson, A. Sobkowiak, S. Lidin, P. Huang, S. Styring, J. Uhlig, J. Bendix, R. Lomoth, V. Sundström, P. Persson and K. Wärnmark, *Nature*, 2017, **543**, 695–699.
9 K. S. Kjær, N. Kaul, O. Prakash, P. Chábera, N. W. Rosemann, A. Honarfar, O. Gordivska, L. A. Fredin, K.-E. Bergquist, L. Häggström, T. Ericsson, L. Lindh, A. Yartsev, S. Styring, P. Huang, J. Uhlig, J. Bendix, D. Strand, V. Sundström, P. Persson, R. Lomoth and K. Wärnmark, *Science*, 2019, **363**, 249–253.
10 L. H. M. de Groot, A. Ilic, J. Schwarz and K. Wärnmark, *J. Am. Chem. Soc.*, 2023, **145**, 9369–9388.
11 A. Ilic, B. R. Strücker, C. E. Johnson, S. Hainz, R. Lomoth and K. Wärnmark, *Chem. Sci.*, 2024, **15**, 12077–12085.
12 J. Wellauer, B. Pfund, I. Becker, F. Meyer, A. Prescimone and O. S. Wenger, *J. Am. Chem. Soc.*, 2025, **147**, 8760–8768.
13 J. D. Braun, I. B. Lozada, C. Kolodziej, C. Burda, K. M. E. Newman, J. van Lierop, R. L. Davis and D. E. Herbert, *Nat. Chem.*, 2019, **11**, 1144–1150.
14 J. D. Braun, I. B. Lozada and D. E. Herbert, *Inorg. Chem.*, 2020, **59**, 17746–17757.
15 C. B. Larsen, J. D. Braun, I. B. Lozada, K. Kunnus, E. Biasin, C. Kolodziej, C. Burda, A. A. Cordones, K. J. Gaffney and D. E. Herbert, *J. Am. Chem. Soc.*, 2021, **143**, 20645–20656.
16 M. E. Reinhard, B. K. Sidhu, I. B. Lozada, N. Powers-Riggs, R. J. Ortiz, H. Lim, R. Nickel, J. V. Lierop, R. Alonso-Mori, M. Chollet, L. B. Gee, P. L. Kramer, T. Kroll, S. L. Raj, T. B. van Driel, A. A. Cordones, D. Sokaras, D. E. Herbert and K. J. Gaffney, *J. Am. Chem. Soc.*, 2024, **146**, 17908–17916.
17 C. Wegeberg, B. K. Sidhu, P. Chábera, J. Uhlig, R. A. Cowin, J. A. Weinstein, P. Persson, A. Yartsev and D. E. Herbert, *Chem. Sci.*, 2025, in revision.
18 M. Chergui and E. Collet, *Chem. Rev.*, 2017, **117**, 11025–11065.
19 L. Velasco, C. Liu, X. Zhang, S. Grau, M. Gil-Sepulcre, C. Gimbert-Suriñach, A. Picón, A. Llobet, S. DeBeer and D. Moonshiram, *ChemSusChem*, 2023, **16**, e202300719.
20 J.-W. Wang, X. Zhang, L. Velasco, M. Karnahl, Z. Li, Z.-M. Luo, Y. Huang, J. Yu, W. Hu, X. Zhang, K. Yamauchi, K. Sakai, D. Moonshiram and G. Ouyang, *JACS Au*, 2023, **3**, 1984–1997.
21 M. Rentschler, S. Iglesias, M.-A. Schmid, C. Liu, S. Tschierlei, W. Frey, X. Zhang, M. Karnahl and D. Moonshiram, *Chem. – Eur. J.*, 2020, **26**, 9527–9536.
22 S. E. Canton, X. Zhang, J. Zhang, T. B. van Driel, K. S. Kjaer, K. Haldrup, P. Chabera, T. Harlang, K. Suarez-Alcantara, Y. Liu, J. Pérez, A. Bordage, M. Pápai, G. Vankó, G. Jennings, C. A. Kurtz, M. Rovezzi, P. Glatzel, G. Smolentsev, J. Uhlig, A. O. Dohn, M. Christensen, A. Galler, W. Gawelda, C. Bressler, H. T. Lemke, K. B. Møller, M. M. Nielsen, R. Lomoth, K. Wärnmark and V. Sundström, *J. Phys. Chem. Lett.*, 2013, **4**, 1972–1976.
23 V. Kabanova, M. Sander, M. Levantino, Q. Kong, S. Canton, M. Retegan, M. Cammarata, P. Lenzen, L. M. D. Lawson and M. Wulff, *Struct. Dyn.*, 2024, **11**, 054901.
24 E. Borfecchia, C. Garino, L. Salassa and C. Lamberti, *Philos. Trans. R. Soc., A*, 2013, **371**, 20120132.
25 C. Adamo and V. Barone, *J. Chem. Phys.*, 1999, **110**, 6158–6170.
26 W. Zhang, R. Alonso-Mori, U. Bergmann, C. Bressler, M. Chollet, A. Galler, W. Gawelda, R. G. Hadt, R. W. Hartsock, T. Kroll, K. S. Kjær, K. Kubiček, H. T. Lemke, H. W. Liang, D. A. Meyer, M. M. Nielsen, C. Purser, J. S. Robinson, E. I. Solomon, Z. Sun, D. Sokaras, T. B. van Driel, G. Vankó, T.-C. Weng, D. Zhu and K. J. Gaffney, *Nature*, 2014, **509**, 345–348.
27 S. Iglesias, A. Gamonal, A. Abudulimu, A. Picón, E. Carrasco, D. Écija, C. Liu, L. Luer, X. Zhang, J. S. Costa and D. Moonshiram, *Chem. – Eur. J.*, 2020, **26**, 10801–10810.
28 J. Wu, M. Alías and C. de Graaf, *Inorganics*, 2020, **8**, 16.
29 P. Chábera, K. S. Kjaer, O. Prakash, A. Honarfar, Y. Liu, L. A. Fredin, T. C. B. Harlang, S. Lidin, J. Uhlig, V. Sundström, R. Lomoth, P. Persson and K. Wärnmark, *J. Phys. Chem. Lett.*, 2018, **9**, 459–463.